

Time-Frequency Analysis of Doppler Radar Signal Using Chirplet Transform

Yuchen Wu*

Department of Applied Science and Engineering
University of Toronto
Toronto, Canada
cheney.wu@mail.utoronto.ca

Yingxue Wang*

Department of Applied Science and Engineering
University of Toronto
Toronto, Canada
yingxue.wang@mail.utoronto.ca

Abstract—Chirplet transform has been proposed as an advanced technique to replace the original Fourier-transformation-based methods in time-frequency analysis. In this project, we studied quadratic and warbling chirp functions, and used quadratic chirplet (“ q -chirplet”) and warble transform to extract certain patterns of frequency from the input signal. In particular, we used the MPLEM algorithm for adaptive chirplet transform, which approximates the input signal with a minimal set of chirplets. We explored the application of chirplet transform in a Doppler radar system as suggested by Mann’s Intelligent Image Processing textbook to detect and analyze certain motion patterns through radar measurements, such as short time constant acceleration and oscillation.

Index Terms—Time-Frequency, Doppler, chirplet, HDR audio, Expectation-Maximization,

I. INTRODUCTION

Time-frequency analysis in applications such as Doppler radar used to be done via short-time Fourier transform (STFT). However, more sophisticated techniques have been developed, notably wavelet transform and chirplet transform. In this project, we investigated chirplet transform that was first introduced by Mann and Haykin [1] in 1991 and later discussed in [2] with connection to Doppler radar systems. We considered two types of chirplets, namely the q -chirplet and warble, and applied chirplet transform to both simulated and real Doppler radar datasets to obtain the motion profile of the measuring target. Using chirplet transform to analyze Doppler radar return is not new. In Mann’s Intelligent Image Processing textbook [3], a Doppler radar vision system based on time-frequency analysis and chirplet transform was proposed and was capable of detecting situations such as car hazard, pickpocket based on the *acceleration intentionality principle*, which suggests that an individual attacker is governed by a fixed degree of acceleration that is changed instantaneously and held roughly constant over a certain time interval. In our experiments, we followed the same design principle in [3] and reproduced some of the key results in it. Moreover, we used adaptive chirplet transform (ACT) techniques, the MPLEM algorithm in particular, to fit the radar data with a minimal set of chirplet bases, which helped filter out noises.

We used both simulated and real Doppler radar data in our experiments. The simulated data include some situations

described in [3], such as stabbing and pickpocket. The real Doppler radar data were collected by Professor Mann using a 24GHz complex-valued Doppler radar system, which include measurements of dropping objects, spinning objects and vibrations of ruler with different length, etc. We show in our experiments that ACT is able to extract key information from the radar signal and detect certain frequency patterns with correspondence to certain motions (e.g. constant short-time acceleration or oscillation) of the measuring target. The source code is available at: <https://github.com/cheneyuwu/ECE516Project>

II. BACKGROUND AND PRELIMINARIES

A. Doppler Radar System

The term “radar vision” was coined by Haykin in 1990, of which the goal is to make radar an intelligent remote-sensing device that is capable of sensing the surrounding environment [4]. A Doppler radar is a specialized radar that uses Doppler effect to produce velocity data about the objects at a distance. By measuring the frequency change between an emitted microwave signal and the returned signal which is bounced back by a desired target, it can obtain an accurate estimate of the object’s motion, such as its radial velocity relative to the radar source. Doppler radar is widely used in many applications such as meteorology, radar guns, sounding satellites and military. Coherent radar systems, meaning the phase relationships between the transmitted and the received pulses are constant, are particularly well suited to Doppler radar signal processing.

B. Logons and the Short-Time Fourier Transform

Motivated by quantum mechanics, in 1946 the physicist Gabor [5] defined elementary time-frequency signals as waveforms that have a minimum spread, governed by Heisenberg’s uncertainty principle in a time-frequency plane (TF plane). He coined these elementary signals as “logons”. To measure time-frequency “information” content, he proposed a decomposition of a signal over a set of logons. This decomposition is now known as the short-time Fourier transform (STFT) [6]. In practice, the procedure for computing STFTs is to divide a signal into short segments of equal length and then compute the Fourier transform separately on each segment, e.g. using a moving window. By collapsing the Fourier spectrum of

*The two authors contributed equally to this project.

each segment, we can obtain a 2-D time-frequency distribution called "spectrogram".

The STFT of a finite energy signal $f(t) \in L^2(\mathbb{R})$ is defined as:

$$Sf(t_c, \omega_c) = \int_{-\infty}^{+\infty} f(t)\omega(t-t_c)e^{-j\omega_c t}dt \quad (1)$$

where $\omega(t-t_c)$ is the moving window. The definition of STFT can be also expressed in the frequency domain as:

$$Sf(t_c, \omega_c) = \frac{1}{2\pi} e^{-j\omega_c t_c} \int_{-\infty}^{+\infty} S(\omega)W(\omega - \omega_c)e^{-j\omega t_c}d\omega \quad (2)$$

where $W(\omega - \omega_c)$ is the Fourier transform of the moving window. Many window functions, such as Hamming, Hanning, Kaiser-Bessel and Gaussian windows are used with each of them for different applications.

The major pitfall of STFT is that it has a fixed resolution. The width of the windowing function relates to how the signal is represented, and we have to trade off between a good frequency resolution or time resolution, due to the constrain of Heisenberg uncertainty principle. It is also isomorphic to the assumption of short-time constant velocity, which requires the velocity to be piece-wise constant. We can do better by modeling the underlying physical phenomena, which leads to the emergence of wavelet transform and chirplet transform techniques.

C. Wavelets and the Wavelet Transform

Logons, previously defined as the elementary signals, may be regarded as "a portion of a wave" or a "wavelet" in a loose sense. The wavelet transform was proposed in 1990s [7] to partially overcome the problem of the fixed resolution with the STFT.

We denote an arbitrary piece of sinusoidal signal resulting from a Gaussian function windowed pure tone as a "wavelet":

$$\psi(t) = \frac{1}{\sqrt{\sqrt{\pi}}} e^{-t^2/2} e^{j\eta t} \quad (3)$$

by setting the time-center to zero and the frequency-center to η , we obtain a mother Gabor "wavelet". Then, a family of "wavelets" can be constructed by successively applying two operations of scale (or time-spread) Δ_t and translation time-center t_c to Eqn. 3.

$$g_{t_c, \Delta_t}(t) = \frac{1}{\sqrt{\Delta_t}} \psi\left(\frac{t-t_c}{\Delta_t}\right) \quad (4)$$

The wavelet transform can then be defined as the inner product between the signal f and wavelets g_{t_c, Δ_t} .

$$Wf(t_c, \Delta_t) = \langle g_{t_c, \Delta_t} | f \rangle = \int_{-\infty}^{+\infty} g_{t_c, \Delta_t}^*(t) f(t) dt \quad (5)$$

Note that the time-center and frequency-center of the wavelet in Eqn. 4 are t_c and $\omega_c = \eta/\Delta_t$. Through the uncertainty principle, one can show that the time-spread Δ_t and the frequency-spread Δ_ω is related by $\Delta_t \Delta_\omega = 1/2$, so that the ratio between the frequency-center and the effective frequency-spread is a constant: $\omega_c/\Delta_\omega = 2\eta$. Therefore, a "wavelet"

acquires narrower time-spread and wider frequency-spread in higher frequency area than in lower frequency area in the TF plane. This property makes wavelet transform suitable for analyzing signals with discontinuity or with abrupt changes, but in the mean time restricts the capability of estimating time-frequency structures of low-frequency signal components with short time-duration, or narrow band, high frequency components.

D. Chirplets and the Chirplet Transform

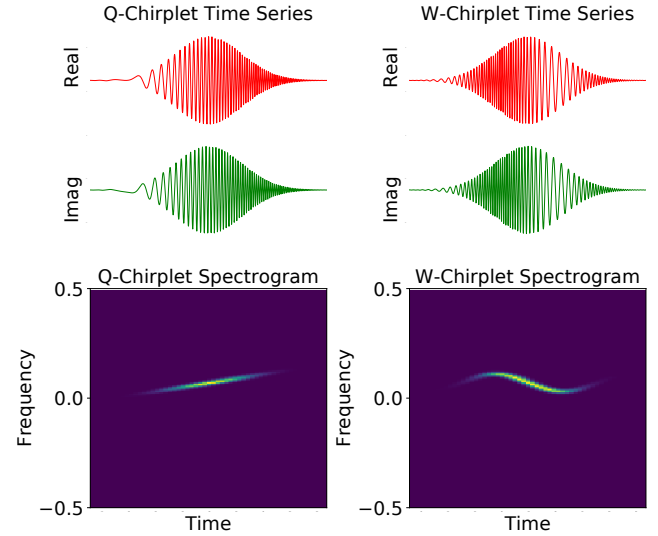


Fig. 1. Example time series of a q -chirplet, a w -chirplet (warble), and their spectrograms. Note that a q -chirplet has a constant frequency rise, thus a straight line pattern is shown in the q -chirplet's spectrogram. A warble has a varying frequency so its spectrogram is curved.

Similar to wavelet, a chirplet is a windowed portion of a chirp function. A chirp, as described in [1], is a sweep signal where the instantaneous frequency varies with time. In this project, we consider quadratic chirp functions (q -chirps) whose instantaneous frequency vary linearly with time, and warbling chirp functions (w -chirps) that have oscillating instantaneous frequency. When using a Gaussian window, a family of chirplets can be constructed by applying mathematical operations to the Gaussian window. In particular, a Gaussian q -chirplet can be represented by

$$g_{t_c, f_c, \Delta_t, c}(t) = \frac{1}{\sqrt{\sqrt{\pi}\Delta_t}} e^{-(1/2)((t-t_c)/\Delta_t)^2} e^{j2\pi[c(t-t_c)^2 + f_c(t-t_c)]} \quad (6)$$

where $j = \sqrt{-1}$. There are 4 parameters in this representation, corresponding to 4 operations in the TF plane:

- t_c : the temporal location of the mean epoch within the time series being analyzed.
- Δ_t : the effective pulse width or *scale*.
- f_c : the mean epoch in Fourier space.
- c : the rate of change of the instantaneous frequency, also known as "chirprate". If chirprate is zero, we have a pure Gabor function.

For w -chirplets (or warblets), we follow the same formulation in [2] that considers a warbling signal whose instantaneous frequency is given by

$$f = \beta \cos(2\pi f_m t + p) + f_c \quad (7)$$

We can integrate Eqn. 7 to get the phase of the warbling chirp, and apply a parameterized Gaussian window to the signal, which leads to the following definition of the family of warblets

$$\begin{aligned} g_{t_c, f_c, \beta, f_m}(t) = \\ \frac{1}{\sqrt{\sqrt{\pi} \Delta_t}} e^{-(1/2)((t-t_c)/\Delta_t)^2} e^{j2\pi[\beta \sin(2\pi f_m t + p)/f_m + f_c(t-t_c)]} \end{aligned} \quad (8)$$

Comparing to the definition of q -chirplets, warblets do not have the chirprate parameter c but introduce another two parameters: the frequency of modulation f_m and the amplitude of modulation β .

Finally, the Gaussian chirplet transform of a signal is the inner product of the signal with a family of Gaussian chirplets (q -chirplets or warblets, etc). It is worth noting that, when analyzing signal from a Doppler radar system, we are particularly interested in certain subspaces of chirplet transform, such as the frequency-frequency (or chirprate-frequency ($c-f_c$)) plane of q -chirplet transform and the dilation-dilation ($f_m-\beta$) plane of warblet-transform as discussed in [2]. These subspaces provide better visualization of the frequency pattern of a signal, as we will show in the experiment section.

E. The Adaptive Chirplet Transform

Adaptive chirplet transform (ACT) aims to find the minimal set of chirplet bases that best approximates a given signal. This technique allows us to process in the "chirplet domain", and convert the estimated signal to time domain as a synthetic process. In a radar system, the fitted individual chirplets help us to understand the different acceleration profiles appearing within the same timing window, thus enable the analysis of multiple objects at the same time. Moreover, since adaptive algorithms only fit the major clusters in the "chirplet domain", noise and non-major information are filtered out and ignored.

Several adaptive approaches have been proposed over the past years. In this project, we mainly considered Matching Pursuit (MP) [8] [9] and Logon Expectation Maximization (LEM) [10]. We implemented the MPLEM algorithm proposed in [11] and used it to analyze the Doppler radar return. We briefly review the MP, LEM and MPLEM algorithm below.

Matching Pursuit (MP)

The MP algorithm approximates a given signal using a sequential estimation scheme. Each time it selects a single chirplet and subtracts it from the signal. More specifically, given a signal $f(t)$, MP first initializes the number of chirplets used to approximate the signal $P = 0$ and the residual $Rf(t) = f(t)$, and then iterates between the following two steps:

Step 1: find the best chirplet from a pre-defined family of chirplets Γ to approximate the current residual

$$\begin{aligned} I_P &= \arg \max_{I \in \Gamma} |\langle g_I | Rf \rangle| \\ a_{I_P} &= \langle g_{I_P} | Rf \rangle \end{aligned} \quad (9)$$

where $I_P = \{t_{cP}, f_{cP}, c_P, \Delta_{tP}\}$ is the collection of the 4 parameters of a Gaussian q -chirplet.

Step 2: update the residual

$$Rf(t) = f(t) - \sum_{p=0}^{P-1} a_{I_p} g_{I_p}(t) \quad (10)$$

and then increment P : $P = P + 1$.

The output of MP is the set of selected chirplets $g_{I_p}, p = 1, \dots, P$, and the approximated signal is then $\sum_{p=1}^P a_{I_p} g_{I_p}$. Regarding about the pre-defined family of chirplets Γ , Bultan [9] proposed a method to discretize the four-parameter space of chirplets while keeping an efficient coverage of the TF. In this project, we also followed his discretization method but only used a subset of the resulting family of chirplets to speed up the overall adaptation process.

Logon Expectation Maximization (LEM)

In contrast to MP, LEM uses a coarse-refinement scheme, which simultaneously estimates a group of chirplets. LEM requires initial guess of the number of chirplets used to approximate the signal as well as a rough estimation of their positions in the TF plane. It then progressively adjusts the chirplets to the true time-frequency structures of the signal. In essence, LEM is an Expectation Maximization algorithm that operates in the TF plane, and the E-step and M-step are defined as follows

E-step:

$$\begin{aligned} e &= f(t) - \sum_{k=0}^{P-1} a_{I_k} g_{I_k}(t) \\ y_k(t) &= a_{I_k} g_{I_k}(t) + \frac{1}{P} e \end{aligned} \quad (11)$$

where P is the number of chirplets and $k = 0, 1, \dots, P - 1$.
M-step:

$$\begin{aligned} I_k &= \arg \max_{I \in \Gamma} |\langle g_{I_k} | y_k \rangle| \\ a_{I_k} &= \langle g_{I_k} | f \rangle \end{aligned} \quad (12)$$

where Γ is again the pre-defined family of chirplets same as in the MP method. Note that the LEM algorithm we described herein is proposed by Cui and Wong [11]. It is different from the original version proposed by Mann and Haykin [10]. This version of LEM uses MP and adjust all four parameters (t_c, f_c, c, Δ_t) of each chirplet. We show the adaptation process of our implementation of LEM in Figure 2.

The MPLEM algorithm

MPLEM simply combines MP and LEM to take advantage from both methods. It uses MP to come up with the initial coarse estimation of the chirplets and then uses LEM to refine the estimation. The pseudo code of MPLEM is shown in Algorithm 1. In our experiments, we applied MPLEM to both

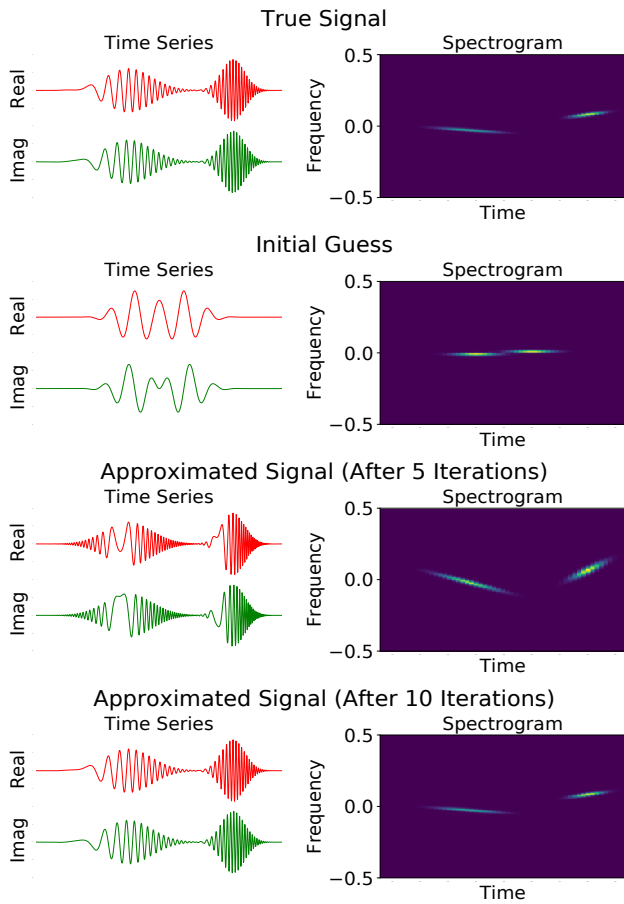


Fig. 2. LEM convergence demonstration. The true signal is a sum of two chirplets with different t_c , f_c , c and Δ_t without noise. We can see that LEM converges very well to the true signal within 10 iterations though the initial guess is not close. For more complex signals, LEM may converge much slower and suffer from non-convergence when a poor initial guess is given.

recorded data from the Doppler radar system and the simulated radar data, and visualized the resulting approximations using spectrograms and the "frequency-frequency" plot introduced in [1].

F. Chirplet Transform with HDR Audio

High Dynamic Range (HDR) composition is a composition technique that extends the dynamic range beyond the native capability of the capturing device. It was first established in the field of image processing by taking images of different exposure levels and combining them to obtain an image that clearly displays both the dark and bright regions. [12] extended this technique to audio and was able to use differently-gained signals to extend the dynamic range to the extreme that beyond the sampling capability of a given analog to digital converter (ADC).

One of the applications of HDR audio is to capture sound from a wearable microphone adjacent to a person's mouth while capturing more distant (i.e. quiet) voices or ambient sounds in the room simultaneously. The previously well known methods like Automatic Gain Control (AGC) is not able to

Algorithm 1 MPLEM [11]

Require: Signal to be approximated $f(t)$, maximum MP iterations M and maximum LEM iterations N

- 1: Initialize MP residual $Rf(t) = f(t)$, $P = 0$
- 2: **for** M iterations **do**
- 3: MP step 1: find the best chirplet to approximate the current residual $Rf(t)$:
- 4: $I_P = \arg \max_{I \in \Gamma} |\langle g_I | Rf \rangle|$
- 5: $a_{I_P} = \langle g_{I_P} | Rf \rangle$
- 6: **for** N iterations **do**
- 7: LEM E-step: compute the approximation error e and targets y_k :
- 8: $e = f(t) - \sum_{k=0}^{P-1} a_{I_k} g_{I_k}(t)$
- 9: $y_k(t) = a_{I_k} g_{I_k}(t) + \frac{1}{P} e$, $k = 0, \dots, P - 1$
- 10: LEM M-step: refine estimation:
- 11: $I_k = \arg \max_{I \in \Gamma} |\langle g_I | y_k \rangle|$, $k = 0, \dots, P - 1$
- 12: $a_{I_k} = \langle g_{I_k} | f \rangle$, $k = 0, \dots, P - 1$
- 13: **end for**
- 14: MP step 2: update the residual:
- 15: $Rf(t) = f(t) - \sum_{p=0}^{P-1} a_{I_p} g_{I_p}(t)$
- 16: $P = P + 1$
- 17: **end for**

handle this situation. If we apply chirplet transform with HDR audio, we open a new window into the world around us. By using the aforementioned time-frequency analysis techniques, for example, we can expand the range of sensing of the Doppler radar system and capture motions of both near-by and rear objects. For example, in Covid-19 detection, we can detect people that are coming far away from us as well as the near-by objects.

III. EXPERIMENT

A. Dataset

In our experiment, we used both simulated Doppler radar data, which were manually generated with added Gaussian noise, and a real-world HDR radar data collected by Professor Mann, which came from a 24GHz *complex-valued Doppler radar system*, to perform time-frequency analysis. The simulated dataset includes a few scenarios described in the "Intelligent Image Processing" textbook by Mann [3], such as *Start Walking*, *Stabbing*, and *Pickpocket*, etc.

The real-world HDR radar dataset consists of complex-valued data (with both real part and imaginary part) of gains $10\times$, $100\times$, $1000\times$, $10000\times$. The dataset includes radar measurements of dropping objects, spinning objects, vibration of rulers, etc.

B. Radar Data Calibration

The given HDR dataset shows the same calibration problems as described in [3] - mirroring in the zero frequency axis, high correlation between the real and imaginary component of the data, and a DC offset give rise to a strong signal at zero frequency, even though there was nothing moving at exactly the same speed as the measuring device.

To calibrate the radar data, we followed the suggestion in [3]: subtract the DC offset inherent in the system, and then compute the inverse of the complex Cholesky factorization of the covariance matrix for the real and imaginary parts, which is then applied to the data. The Cholesky decomposition of a Hermitian positive-definite matrix \mathbf{A} is a decomposition of the form

$$\mathbf{A} = \mathbf{L}\mathbf{L}^* \quad (13)$$

where \mathbf{L} is a lower triangular matrix with real and positive diagonal entries, and \mathbf{L}^* denotes the conjugate transpose of \mathbf{L} .

Figure 3 shows the correlation between the real and imaginary component of the *dropping 1 object* radar data before and after calibration as well as the corresponding spectrograms. Notice that after calibration (the right column in Figure 3), the constant DC offset is removed and the data approximately forms an isotropic circular blob centered at the origin.

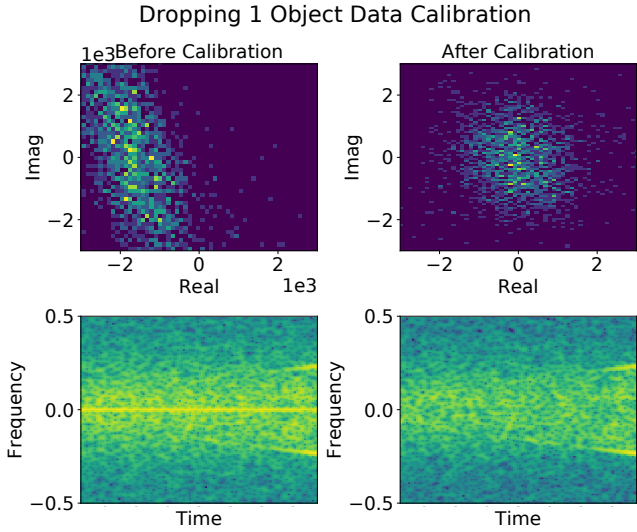


Fig. 3. Data distribution before and after Cholesky factorization of the *dropping 1 object* data with 1000 samples. Notice the obvious correlation of the imaginary and real component, suggested by the data scattering along the diagonal line of the imaginary-versus-real plot. Also notice the calibrated data forms an approximately isotropic circular blob centered at the origin. The DC offset around 0 frequency is removed through calibration.

C. Detecting Short-Time Constant Acceleration via Q-Chirplet Transform

We evaluate the performance of the MPLEM algorithm for ACT on both simulated radar data (Figure 4) and the collected HDR radar data (Figure 5). We observed that ACT is capable of recovering the dominate information exists in the signal, and ignore the environment noise. However, it may eliminate some weak signals when operating in a real-world scenario. Moreover, the bowtie patterns resulting from ACT is distinguishable and clearly represents the acceleration information.

D. Detecting Oscillation via Warblet Transform

We also applied Warblet (w-chirplet) transform to the collected warbling radar data as well as a simulated composite

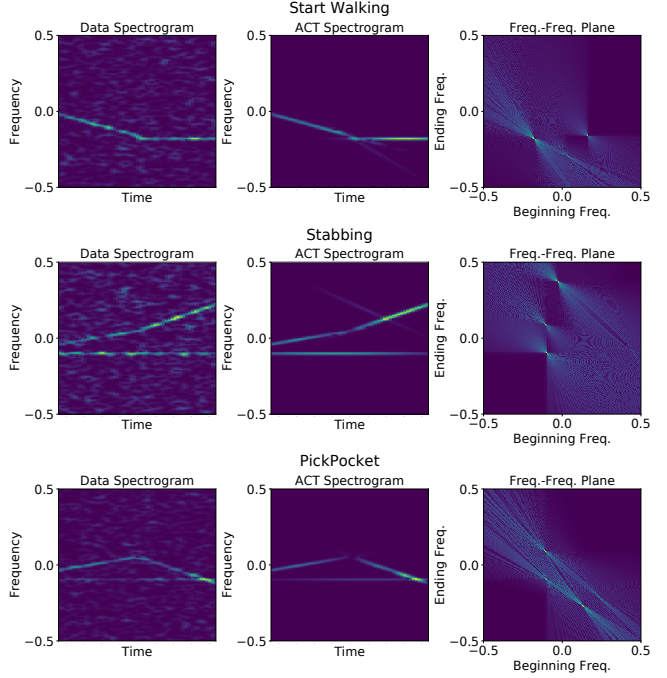


Fig. 4. Adaptive Chirplet Transform on simulated data for "Start Walking", "Stabbing", and "Pickpocket" actions. The data are manually generated with added Gaussian noise, whose spectrograms are shown in the left-most column. The mid-column is the estimated signals using MPLEM. Notice that MPLEM fully recovered the information in the simulated data and ignored the noise. The right column shows the bowtie plots for the estimated data. Each bowtie center corresponds to a line segment in the spectrogram. For example, in the "Start Walking" data, the right bowtie matches the descending segment, and the left one matches the flat (constant frequency) segment.

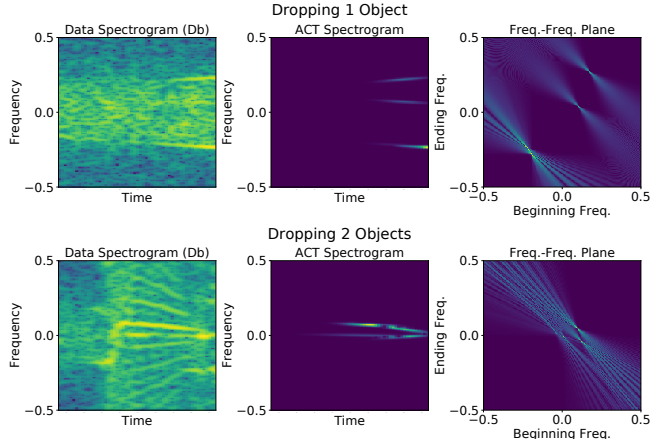


Fig. 5. Adaptive Chirplet Transform on calibrated *dropping 1 object* and *dropping 2 objects* data with 1000 samples. Notice there are a lot of noise in the spectrogram of the collected radar data shown in the left-most column, so that we plot the spectrogram in Db scale. By applying MPLEM, we were able to recover the major components of the original spectrogram, eliminate noise and maybe some weak information as well. The resulting bowtie plots from the ACT-generated spectrogram is shown on the right-most column, which is clear an noise-free. However, unfortunately we were not able to detect the dropping objects well from the radar signals due to the noises. From the *dropping 1 object* data, we can see mirroring in the zero frequency axis, so that MPLEM extracts signal with both increasing and decreasing frequency.

signal, as shown in Figure 6 and 7. We present the signals in TF plane and observe sinusoidal patterns of different frequencies. The resulting dilation-dilation subspaces, computed with a warbling mother chirplet, is an intensity map that shows the location of where the signal peaks in the modulation index ("amplitude of modulation") versus modulation frequency plane.

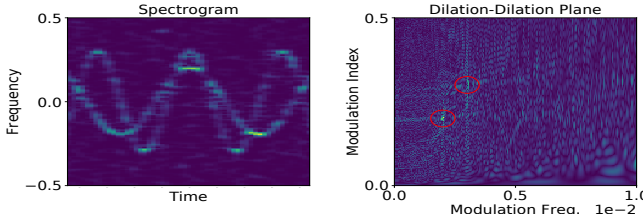


Fig. 6. Warble transform applied to simulated radar data. The two sinusoidal patterns of different frequency in the time-frequency distribution each corresponds to the peaks (bright clusters) residing in the dilation-dilation plane, which are circled in red. The peak with lower modulation frequency corresponds to the slower-changing pattern in the spectrogram.

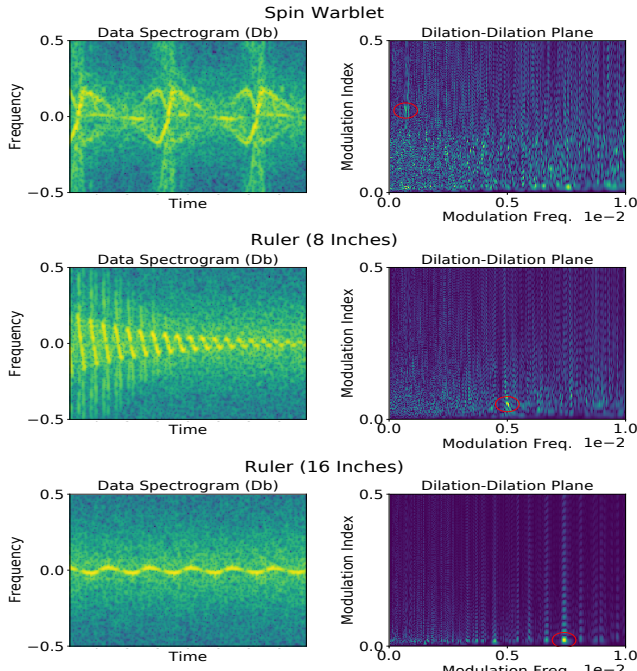


Fig. 7. Warble transform applied to the collected radar data with 4000 samples. Notice that there is a peak in the very low modulation frequency region from the pattern in the dilation-dilation plane of the *Spin Warble* data, which agrees with the slow oscillating pattern in the spectrogram. In the *Ruler (8 Inches)* data, we can see sinusoidal patterns in the spectrogram, corresponding to the circled bright clusters in the dilation plane. However, for the *Ruler (16 Inches)* data, it is misleading that the time-frequency pattern with lower sinusoidal frequency than *Ruler (8 Inches)* results in a peak at higher modulation frequency.

IV. CONCLUSION

In this project, we reviewed the history of time-frequency analysis, and studied the quadratic and warbling chirplet functions. We applied an ACT algorithm, MPLEM, to simulated

radar signals as well as real radar data collected from a complex-valued Doppler radar system. MPLEM can approximate the input signal with a minimal set of chirplets fairly well, and were able to remove the noisy components. However, it may overlook the weak but useful information presented in the collected radar data. Further, we were able to extract target object's acceleration profile with q -chirplet transform using the clean, estimated signals regenerated by ACT, and obtain results that agree with the spectrograms. We also experimented with warble transform and tried to obtain the oscillation pattern of spinning or vibrating objects. The warble transform only resulted in less-informative dilation-dilation plots due to the large amount of noise in the real-world radar data, as suggested in the time-frequency plots.

As previously mentioned in section II-F, we can apply chirplet transform to HDR radar data in order to obtain a better sensing capability of multiple objects' motion profiles appearing concurrently in a scene. We also observed that ACT is capable of recovering the signal waveforms and removing noise in radar data. Therefore, an interesting future work is to find a way to composite the HDR information efficiently, so that ACT can be applied to estimate the signals and we can visualize the motion profiles of multiple objects within the scene. Such technique will serve well in radar detection applications, especially when being applied to the complex real-world scenarios.

REFERENCES

- [1] Mann, Steve and Haykin, Simon, "The chirplet transform: A generalization of Gabor's logon transform," *Vision Interface '91*, pp. 205–212, June 3-7 1991, iSSN 0843-803X.
- [2] Steve Mann and Simon Haykin, "The chirplet transform: Physical considerations," *IEEE Trans. Signal Processing*, vol. 43, no. 11, pp. 2745–2761, November 1995.
- [3] S. Mann, *Where on the Body is the Best Place for a Personal Imaging System?* John Wiley & Sons, Ltd, 2002, ch. 2, pp. 15–63. [Online]. Available: <https://onlinelibrary.wiley.com/doi/abs/10.1002/0471221635.ch2>
- [4] S. Haykin, "Radar vision," in *IEEE International Conference on Radar*, 1990, pp. 585–588.
- [5] D. Gabor, "Theory of communication. Part 1: The analysis of information," *Journal of the Institution of Electrical Engineers - Part III: Radio and Communication Engineering*, vol. 93, no. 26, pp. 429–441, Nov. 1946. [Online]. Available: <https://digital-library.theiet.org/content/journals/10.1049/ji-3-2.1946.0074>
- [6] E. Sejdić, I. Djurović, and J. Jiang, "Time-frequency feature representation using energy concentration: An overview of recent advances," *Digital Signal Processing*, vol. 19, no. 1, pp. 153–183, Jan. 2009. [Online]. Available: <https://linkinghub.elsevier.com/retrieve/pii/S105120040800002X>
- [7] S. Mallat, *A Wavelet Tour of Signal Processing*. Burlington: Elsevier, 1999, oCLC: 476114751. [Online]. Available: <https://public.ebookcentral.proquest.com/choice/publicfullrecord.aspx?p=319092>
- [8] S. G. Mallat and Zhifeng Zhang, "Matching pursuits with time-frequency dictionaries," *IEEE Transactions on Signal Processing*, vol. 41, no. 12, pp. 3397–3415, 1993.
- [9] A. Bultan, "A four-parameter atomic decomposition of chirplets," *IEEE Transactions on Signal Processing*, vol. 47, no. 3, pp. 731–745, 1999.
- [10] Mann, Steve and Haykin, Simon, "The Adaptive Chirplet: An Adaptive Wavelet Like Transform," *SPIE, 36th Annual International Symposium on Optical and Optoelectronic Applied Science and Engineering*, 21-26 July 1991.
- [11] R. Cui and W. Wong, "The adaptive chirplet transform and visual evoked potentials," *IEEE transactions on bio-medical engineering*, vol. 53, pp. 1378–84, 08 2006.

- [12] R. Janzen and S. Mann, "High dynamic range simultaneous signal compositing, applied to audio," in *Electrical & Computer Engineering (CCECE), 2012 25th IEEE Canadian Conference on*. IEEE, 2012, pp. 1–6.